

Interleukin-6/interleukin-21 signaling axis is critical in the pathogenesis of pulmonary arterial hypertension

Takahiro Hashimoto-Kataoka^a, Naoki Hosen^b, Takashi Sonobe^c, Yoh Arita^a, Taku Yasui^a, Takeshi Masaki^a, Masato Minami^d, Tadakatsu Inagaki^c, Shigeru Miyagawa^e, Yoshiki Sawa^e, Masaaki Murakami^f, Atsushi Kumanogoh^g, Keiko Yamauchi-Takahara^a, Meinoshin Okumura^d, Tadimitsu Kishimoto^h, Issei Komuro^{ij}, Mikiyasu Shirai^c, Yasushi Sakata^a, and Yoshikazu Nakaoka^{a,k,1}

Departments of ^aCardiovascular Medicine, ^bCancer Stem Cell Biology Functional Diagnostic Science, ^dGeneral Thoracic Surgery, ^eCardiovascular Surgery, and ^gRespiratory Medicine, Allergy and Rheumatic Disease, Osaka University Graduate School of Medicine, Suita, Osaka, 565-0871, Japan; ^cDepartment of Cardiac Physiology, National Cerebral and Cardiovascular Center Research Institute, Suita, Osaka, 565-8565, Japan; ^fDepartment of Molecular Neuroimmunology, Institute for Genetic Medicine, Hokkaido University, Sapporo, Hokkaido, 060-0815, Japan; ^hLaboratory of Immune Regulation, Immunology Frontier Research Center, Osaka University, Suita, Osaka, 565-0871, Japan; ⁱDepartment of Cardiovascular Medicine, The University of Tokyo Graduate School of Medicine, Tokyo, 113-8656, Japan; and ^jCore Research for Evolutional Science and Technology and ^kPrecursory Research for Embryonic Science and Technology, Japan Science Technology Agency, Kawaguchi, Saitama, 332-0012, Japan

Edited by Kari Alitalo, University of Helsinki, Helsinki, Finland, and approved April 16, 2015 (received for review December 26, 2014)

IL-6 is a multifunctional proinflammatory cytokine that is elevated in the serum of patients with pulmonary arterial hypertension (PAH) and can predict the survival of patients with idiopathic PAH (IPAH). Previous animal experiments and clinical human studies indicate that IL-6 is important in PAH; however, the molecular mechanisms of IL-6-mediated pathogenesis of PAH have been elusive. Here we identified IL-21 as a downstream target of IL-6 signaling in PAH. First, we found that IL-6 blockade by the monoclonal anti-IL-6 receptor antibody, MR16-1, ameliorated hypoxia-induced pulmonary hypertension (HPH) and prevented the hypoxia-induced accumulation of Th17 cells and M2 macrophages in the lungs. Consistently, the expression levels of IL-17 and IL-21 genes, one of the signature genes for Th17 cells, were significantly up-regulated after hypoxia exposure in the lungs of mice treated with control antibody but not in the lungs of mice treated with MR16-1. Although IL-17 blockade with an anti-IL-17A neutralizing antibody had no effect on HPH, IL-21 receptor-deficient mice were resistant to HPH and exhibited no significant accumulation of M2 macrophages in the lungs. In accordance with these findings, IL-21 promoted the polarization of primary alveolar macrophages toward the M2 phenotype. Of note, significantly enhanced expressions of IL-21 and M2 macrophage markers were detected in the lungs of IPAH patients who underwent lung transplantation. Collectively, these findings suggest that IL-21 promotes PAH in association with M2 macrophage polarization, downstream of IL-6-signaling. The IL-6/IL-21-signaling axis may be a potential target for treating PAH.

pulmonary arterial hypertension | interleukin-21 | interleukin-6 | Th17 cells | M2 macrophage

Pulmonary arterial hypertension (PAH) is a debilitating disease characterized by arteriopathy in the small to medium-sized distal pulmonary arteries that is associated with arterial muscularization, concentric intimal thickening, and the formation of plexiform lesions (1, 2). Inflammation and autoimmunity currently are recognized as critical contributors to the pathogenesis of PAH (3, 4). Inflammatory cells such as T cells, B cells, and macrophages infiltrate the plexiform lesions in patients with advanced PAH. Thus, proinflammatory cytokines produced by these cells may be responsible for the hyperproliferation of pulmonary artery endothelial cells (PAECs) and pulmonary artery smooth muscle cells (PASCs) (5, 6).

IL-6 is a multifunctional proinflammatory cytokine linked to numerous autoimmune diseases (7, 8). Patients with idiopathic PAH (IPAH) exhibit increased IL-6 serum levels, which correlate with their prognoses (3, 9, 10). Consistent with these findings, lung-specific IL-6 transgenic mice display spontaneous pulmonary hypertension in normoxia and develop greatly exaggerated hypoxia-induced pulmonary hypertension (HPH) (11), whereas IL-6–

deficient mice show resistance to HPH (12). These findings suggest that IL-6 has a significant role in the pathogenesis of pulmonary hypertension; however, the downstream target(s) of IL-6 in HPH have been elusive.

T-helper cells are comprised of three subsets, Th1, Th2, and Th17 cells, which are defined by the cytokines they produce (13, 14). Th17 cells, a subset of IL-17–producing effector T cells, play important roles in the pathogenesis of autoimmune diseases such as rheumatoid arthritis (13, 14). IL-6 together with TGF- β promotes the differentiation of Th17 cells (14, 15). However, the involvement of Th17 cells in the pathogenesis of HPH has not been determined.

Macrophages undergo differential polarization that generates three distinct macrophage populations: the classically activated (M1), alternatively activated (M2), and anti-inflammatory (regulatory) macrophages (16–18). Upon their activation by IFN- γ and TNF- α , M1 macrophages exert microbicidal and tumoricidal effects by producing inducible nitric oxide synthase and IL-12p40

Significance

Pulmonary arterial hypertension (PAH) is a serious disease characterized by vascular remodeling in pulmonary arteries. Although an elevated IL-6 serum level correlates with poor prognosis of PAH patients, it is unclear how IL-6 promotes PAH. Here we identified IL-21 as a downstream target of IL-6 signaling in PAH. In mice with hypoxia-induced pulmonary hypertension (HPH), Th17 cells and M2 macrophages accumulate in the lungs after hypoxia exposure. IL-21 primarily derived from Th17 cells promotes M2 macrophage polarization. Consistently, IL-21 receptor-deficient mice show resistance to HPH with no accumulation of M2 macrophages in the lungs. IL-21 and M2 macrophage markers were upregulated in the lungs of patients with end-stage idiopathic PAH. These findings suggest promising therapeutic strategies for PAH targeting IL-6/IL-21-signaling axis.

Author contributions: T.H.-K., T.K., I.K., M.S., and Y.N. designed research; T.H.-K., N.H., T.S., Y.A., T.Y., T.M., M. Minami, T.I., S.M., K.Y.-T., M.S., and Y.N. performed research; M. Minami, Y. Sawa, M. Murakami, M.O., and T.K. contributed new reagents/analytic tools; T.H.-K., N.H., T.S., M. Murakami, A.K., K.Y.-T., M.S., Y. Sakata, and Y.N. analyzed data; and T.H.-K. and Y.N. wrote the paper.

Conflict of interest statement: T.K. holds a patent for a monoclonal humanized anti-IL6R antibody (tocilizumab). Y.N. is a consultant of the sponsor-initiated clinical trial (Chugai Pharmaceutical Co.) using tocilizumab for Takayasu arteritis.

This article is a PNAS Direct Submission.

Freely available online through the PNAS open access option.

¹To whom correspondence should be addressed. Email: ynakaoka@cardiology.med.osaka-u.ac.jp.

This article contains supporting information online at www.pnas.org/lookup/suppl/doi:10.1073/pnas.1424774112/-DCSupplemental.

(17, 18). In contrast, M2 macrophages are activated by IL-4 and IL-13 and characteristically express arginase-1 (Arg1), found in inflammatory zone-1 (Fizz1), chitinase 3-like-3 (Ym1), and mannose receptor, C type lectin-1 (MRC-1) (16–18). Intriguingly, M2 macrophages recently were reported to play a critical role in HPH (19); however, the molecular mechanisms underlying macrophage polarization in HPH are unknown.

Here, we examined the roles of IL-6 and its downstream signaling targets in the pathogenesis of HPH in mice. We found that the IL-6/IL-21–signaling axis played critical roles in the development of HPH in association with M2 macrophage polarization. Consistent with these findings in mice, large numbers of IL-21⁺ cells and M2 macrophages were detected in the lungs of patients with IPAH. Taken together, these findings indicate a conserved role for the IL-6/IL-21–signaling axis in mouse HPH and human PAH (HPAH) and suggest promising targets for treating PAH.

Results

Hypoxia-Induced IL-6 Expression in Mouse Pulmonary Vessels. We first examined the *Il-6* mRNA levels in the lungs of C57BL/6 mice after hypoxia exposure using quantitative RT-PCR (qRT-PCR). The *Il-6* mRNA levels peaked on day 2 and returned to basal levels by day 7 after hypoxia exposure (Fig. 1A). Consistent with this finding, immunohistochemical analysis demonstrated strong IL-6 induction in the intima and medial layers of the arterioles and small arteries of the lung on day 2 after hypoxia exposure (Fig. 1B).

IL-6 Blockade by MR16-1 Prevents HPH. IL-6 signaling is transduced primarily by STAT3. Thus, we examined the tyrosine-phosphorylation of STAT3 in the lungs of mice. Although tyrosine-phosphorylation of STAT3 was strongly induced by hypoxia exposure in the lungs of mice treated with control antibody, it was attenuated in those treated with the anti-IL-6 receptor (IL-6R) antibody MR16-1 (Fig. 1C). Next, we investigated the effect of IL-6 blockade on HPH development by measuring the right ventricular systolic pressure (RVSP), Fulton’s index [right/(left +

septum) ventricular weight], and the medial wall thickness index, which is estimated by elastic Van Gieson staining of the pulmonary arterioles (Fig. 1D). In control antibody-treated mice, hypoxia exposure for 4 wk induced significant increases in the RVSP, Fulton’s index, and medial wall thickness index, compared with the values observed under normoxic conditions (Fig. 1E–G). In contrast, the hypoxia-induced elevation of these parameters was significantly inhibited by treatment with MR16-1 (Fig. 1E–G). Similarly, thickened medial vascular walls were detected in the lung sections of control antibody-treated mice but not in those of mice treated with MR16-1 (Fig. 1H). Under normoxia, there was no significant difference in the physiological parameters of mice treated with control antibody and those treated with MR16-1 (Table S1). These data suggest that IL-6 blockade by MR16-1 effectively prevents HPH.

IL-6 Blockade Abrogates Hypoxia-Induced Accumulation of Th17 Cells in the Lungs. IL-6–dependent accumulation of Th17 cells promotes the development of inflammatory diseases, such as rheumatoid arthritis (20). Thus, we examined the involvement of Th17 cells in HPH by measuring the mRNA levels of *Il-17A*, a Th17 signature gene. Hypoxia-induced *Il-17A* in the lungs peaked on day 2 and declined on day 7 but remained slightly higher than the basal level on and after day 7 (Fig. 2A). We next examined the mRNA levels of *Il-17A* and other Th17 signature gene, such as *Rorc* (retinoic acid receptor–related orphan receptor-c, also known as “*Ror-γt*”), and IL-17–downstream chemokines, such as *Cxcl1* and *Cxcl5*, in the lungs of mice exposed to hypoxia for 2 d. The mRNA levels of all these genes were significantly up-regulated in the lungs of control antibody-treated mice but not in those of mice treated with MR16-1 (Fig. 2B–E). The IL-17A protein levels also were increased after hypoxia in the lungs of control antibody-treated mice but not in those of mice treated with MR16-1 (Fig. 2F and G). In addition, exposure to hypoxia for 3 d led to significantly increased Th17 numbers in the lungs of control antibody-treated mice but not in those of mice treated with MR16-1 (Fig. 2H and I). In contrast, there was no substantial difference in Th1 and Th2 numbers in the lungs of mice

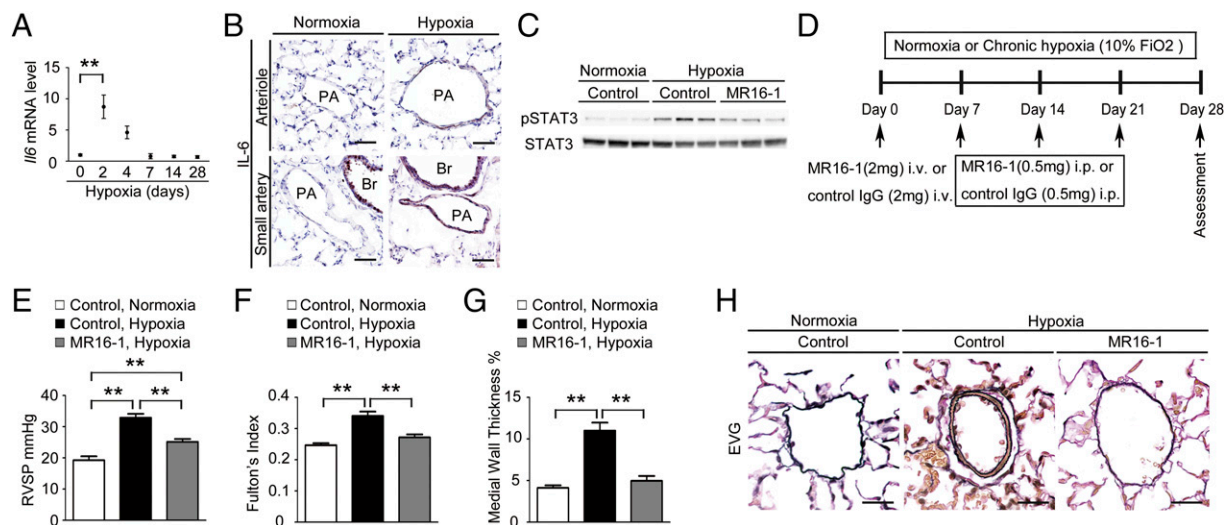


Fig. 1. Blockade of IL-6 signaling prevents HPH. (A) qRT-PCR analysis of *Il-6* mRNA expression in the lungs of C57BL/6 WT mice after hypoxia exposure. Each data point represents the analysis of 5–10 mice. (B) Representative IL-6 immunostaining of lung sections from C57BL/6 mice after exposure to hypoxia or normoxia for 2 d ($n = 5$). (C) Western blot analysis of STAT3 phosphorylation (Tyr705) and total STAT3 in lung homogenates from mice treated with control antibody or MR16-1 after exposure to normoxia or hypoxia for 2 d ($n = 3$). (D) Experimental protocol for examining the effect of antibody treatment on HPH. MR16-1 or control antibody was administered to C57BL/6 mice under normoxic or hypoxic conditions. (E–G) Assessment of antibody-treated mice. (E) RVSP ($n = 8–12$). (F) Fulton’s index ($n = 8–12$). (G) Medial wall thickness index (percent wall thickness) ($n = 5–6$). Distal acinar arterioles (50–100 μm in diameter) were examined. (H) Representative images of the vascular remodeling of distal acinar arterioles in lung sections subjected to elastic Van Gieson (EVG) staining. (Scale bars: 25 μm .) Br, bronchus; PA, pulmonary artery. Values shown are the mean \pm SEM; * $P < 0.05$, ** $P < 0.01$ calculated using ANOVA.

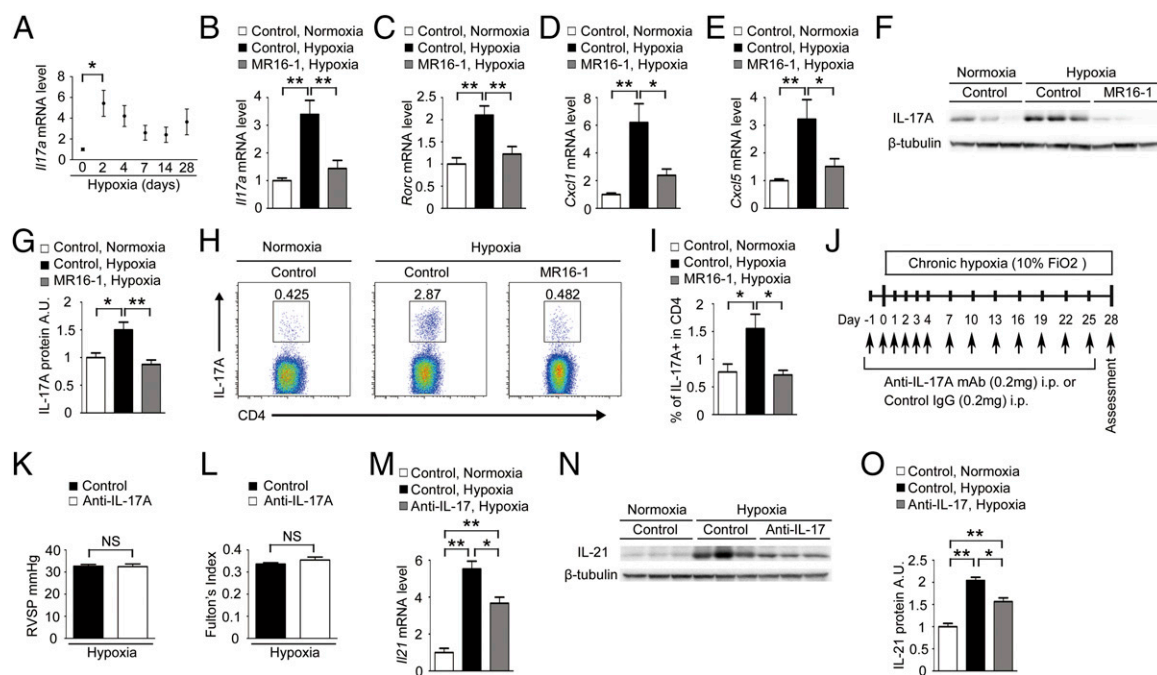


Fig. 2. IL-6 blockade inhibits accumulation of Th17 cells in the murine lung after hypoxia exposure. (A) qRT-PCR analysis of *Il-17A* mRNA expression in the lungs of C57BL/6 WT mice after hypoxia exposure. The results are pooled data from at least three independent experiments with 5–10 mice per group. (B–E) qRT-PCR analysis of *Il-17A* (B), *Rorc* (C), *Cxcl1* (D), and *Cxcl5* (E) mRNA expression in the lungs of mice treated with control antibody or MR16-1 after exposure to hypoxia or normoxia for 2 d ($n = 8$). (F and G) Western blot analysis of IL-17A in the lung homogenates from mice treated with control antibody or MR16-1 after exposure to hypoxia or normoxia for 2 d ($n = 6$). Relative levels of IL-17A protein (normalized to β -tubulin) compared with the normoxic control group are shown. (H) Flow cytometric analysis of IL-17A-expressing cells in the CD4⁺ gated T-cell population isolated from the lungs of mice treated with control antibody or MR16-1 after exposure to hypoxia or normoxia for 3 d ($n = 6$). (I) Percentage of IL-17A⁺ cells within the CD4⁺ population. Values shown are the mean \pm SEM; * $P < 0.05$, ** $P < 0.01$ calculated using ANOVA. (J) Experimental protocol for examining the effect of anti-IL-17A antibody treatment on HPH. An anti-IL-17A neutralizing monoclonal antibody or control antibody (IgG) was administered to C57BL/6 mice under hypoxic conditions. (K and L) Assessment of antibody-treated mice. RVSP ($n = 6$) (K) and Fulton's index ($n = 6$) (L) are shown. (M–O) IL-17A blockade significantly attenuates the hypoxia-induced IL-21 up-regulation in the murine lungs. (M) qRT-PCR analysis of *Il-21* mRNA expression in the lungs of mice treated with control antibody or an anti-IL-17A neutralizing antibody after exposure to hypoxia or normoxia for 2 d ($n = 3$). (N and O) Western blot analysis of IL-21 in the lung homogenates from mice treated with control antibody or an anti-IL-17A neutralizing antibody after exposure to hypoxia or normoxia for 2 d ($n = 3$). Values shown are the mean \pm SEM; * $P < 0.05$, ** $P < 0.01$ calculated using ANOVA. NS, not significant.

treated with control antibody or with MR16-1 exposed to hypoxia (Fig. S1). These findings suggest that IL-6 is critical for the hypoxia-induced accumulation of Th17 cells in the lungs.

We next examined the effect of IL-17 blockade on HPH (Fig. 2J). Treatment with an anti-IL-17A neutralizing antibody had no inhibitory effect on the hypoxia-induced elevation in RVSP and Fulton's index compared with control antibody treatment, indicating that IL-17 is not required for HPH development (Fig. 2K and L).

IL-6 Blockade Suppresses the Hypoxia-Induced Accumulation of IL-21-Producing Th17 Cells in the Lungs. IL-21 is an IL-2 family cytokine produced by activated T cells, including Th17 cells, that regulates immune responses (21). We found that the *Il-21* mRNA level peaked on day 2, remained elevated until day 14, and returned to the basal levels on day 28 after hypoxia exposure (Fig. 3A). Hypoxia induced a significantly up-regulated *Il-21* mRNA level in the lungs of mice treated with control antibody but not in the lungs of mice treated with MR16-1 (Fig. 3B). Similarly, hypoxia-induced IL-21 protein levels were increased significantly in the lungs of mice treated with control antibody but not in those treated with MR16-1 (Fig. 3C and D). In addition, hypoxia induced significantly increased numbers of Th17 cells, which produce both IL-17 and IL-21, in the lungs of mice treated with control antibody but not in those treated with MR16-1 (Fig. 3E–G). These findings suggest that IL-6 promotes the accumulation of IL-21-producing Th17 cells in the lungs after hypoxia exposure.

We also examined the effect of IL-17A blockade with anti-IL-17A neutralizing antibody on the level of IL-21 expression in the lungs after hypoxia exposure. IL-17A blockade significantly attenuated hypoxia-induced up-regulation of IL-21 in the lungs of mice after hypoxia exposure (Fig. 2M–O). These findings suggest that IL-17 is in part involved in the hypoxia-induced up-regulation of IL-21.

IL-21 Receptor Knockout Mice Are Resistant to HPH. We next evaluated the effect of hypoxia on IL-21 receptor (IL-21R) knockout (IL-21RKO) mice (Fig. 3H) (22). WT mice exposed to hypoxia for 4 wk exhibited significantly increased RVSP, Fulton's index, and medial wall thickness compared with mice exposed to normoxia (Fig. 3I–K). In contrast, the hypoxia-induced elevation of these parameters was inhibited significantly in IL-21RKO mice (Fig. 3I–K). Similarly, remodeling of the medial vascular walls following hypoxia exposure in WT mice also was inhibited significantly in the lungs of IL-21RKO mice (Fig. 3L). WT and IL-21RKO mice showed no differences in physiological parameters under normoxia (Table S2). These findings suggest that IL-21R-deficient mice are resistant to HPH.

IL-6 Blockade Inhibits the Hypoxia-Induced Generation of M2 Macrophages in the Lung. Alveolar macrophages undergo M2 macrophage polarization in response to hypoxia (19). Therefore, we examined the effect of MR16-1 treatment on the macrophage polarization in the lungs after hypoxia exposure. First, we examined a temporal profile of cell

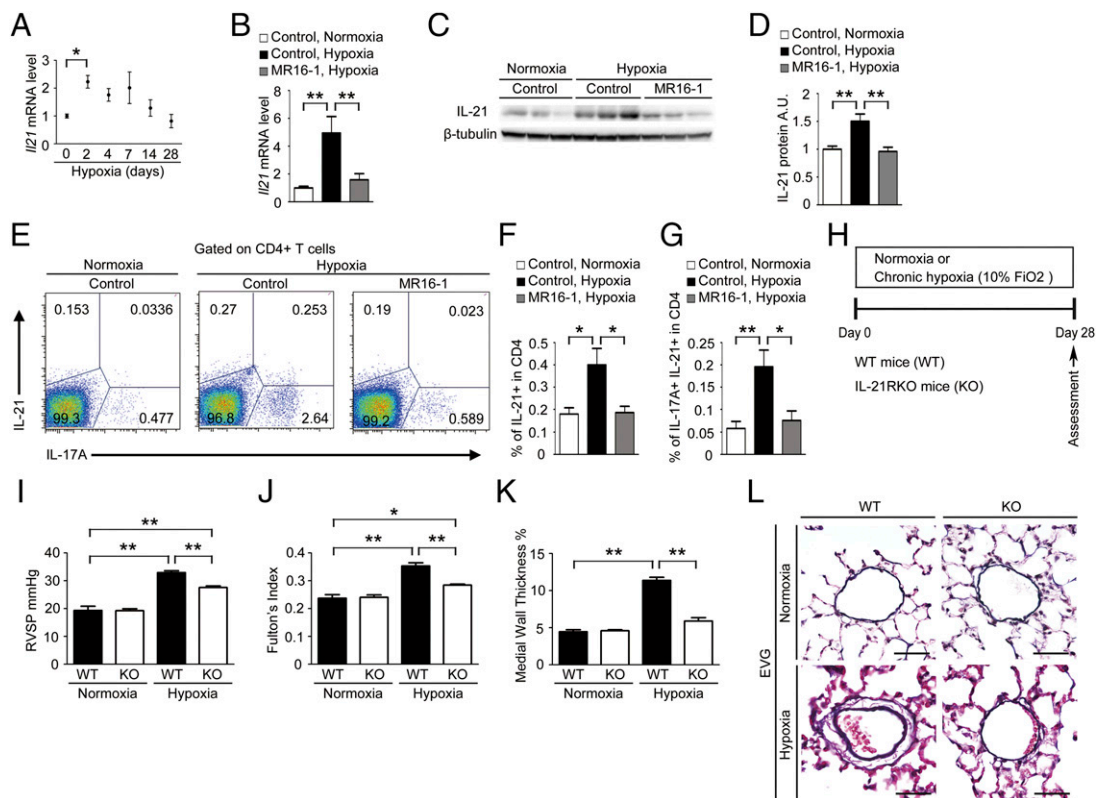


Fig. 3. IL-21, a downstream target of IL-6, mediates the development of HPH in mice. (A) qRT-PCR analysis of *Il-21* mRNA expression in the lungs of C57BL/6 WT mice after hypoxia exposure. The results are pooled data from at least three independent experiments with 5–10 mice per group. (B) qRT-PCR analysis of *Il-21* mRNA expression in the lungs of mice treated with control antibody or MR16-1 after exposure to hypoxia or normoxia for 2 d ($n = 8$). (C and D) Relative levels of IL-21 protein (normalized to β -tubulin) compared with the normoxic control group. A.U., arbitrary units. (E) Flow cytometric analysis of IL-17A⁺/IL-21⁺ cells in the CD4⁺ gated T-cell population isolated from the lungs of mice treated with control antibody or MR16-1 after exposure to hypoxia or normoxia for 3 d ($n = 6$). (F and G) Percentage of IL-21⁺ (F) and IL-17A⁺/IL-21⁺ cells (G) within the CD4⁺ population. (H) Experimental protocol for examining the effect of IL-21R deficiency on HPH. (I–K) Assessment of WT and IL-21RKO (KO) mice. RVSP ($n = 5–10$) (I), Fulton's index ($n = 5–10$) (J), and percent wall thickness ($n = 5$) (K) are shown. Distal acinar arterioles (50–100 μ m in diameter) were examined. (L) Representative images of vascular remodeling of the distal acinar arterioles, subjected to elastic Van Gieson staining. (Scale bar: 40 μ m.) Values shown are the mean \pm SEM; * $P < 0.05$, ** $P < 0.01$ calculated using ANOVA.

content in the bronchoalveolar lavage fluid (BALF) of C57BL6 mice after hypoxia exposure. The percentage of the CD45⁺CD11c⁺F4/80⁺ cells in the BALF-isolated living cells was $83.7 \pm 0.7\%$ by flow cytometry analysis (Fig. S2A and B). The percentage of the alveolar macrophage lineage (CD11c⁺F4/80⁺) cells in the CD45⁺ cells was $92.4 \pm 0.9\%$ (Fig. S2C). The mRNA levels of *Fizz1* (also known as “*Relma*, *resistin-like molecule- α* ”), an M2 signature gene, in the alveolar macrophages isolated from the BALF of C57BL6 mice after hypoxia exposure peaked on day 4, were declining on day 7, but remained elevated until day 14 after hypoxia exposure (Fig. 4A), indicating that the hypoxia-induced M2 macrophage accumulation in the lung occurred 2 d later than the increase of IL-6 and IL-21 on day 2.

Next, we examined the mRNA levels of *Fizz1* and other M2 signature genes, including *Arg1* (arginase 1), *Chi3l3* (chitinase 3-like 3), *Mrc1* (mannose receptor, C type 1) and *Cxcl12* (also known as “*Sdf1*”) in the alveolar macrophages isolated from the BALF after mice were exposed to hypoxia for 4 d. Hypoxia induced significant M2 signature gene up-regulation in the mice treated with control antibody but not in those treated with MR16-1 (Fig. 4B–F). Similarly, hypoxia exposure for 1 wk induced a significant up-regulation of *Fizz1* protein levels in the lungs of mice treated with control antibody but not in those of mice treated with MR16-1, as shown by Western blot (Fig. 4G and H) and immunohistochemical (Fig. 4I and J) analyses. In contrast, there were no significant differences in the mRNA levels of M1 signature genes, including *Nos2* (also known as

“*iNos*”), *Il-12 β* (*Il-12p40*), and *Tnf- α* , in control- and MR16-1-treated mice following hypoxia exposure (Fig. S3A–C). Notably, treatment with IL-6, soluble IL-6R (sIL-6R), or both IL-6 and sIL-6R had no effect on either M1 or M2 signature gene expression in the alveolar macrophages isolated from BALF (Fig. S4). Collectively, these data indicate that IL-6 indirectly promotes the hypoxia-induced generation of M2 macrophages in the lungs.

IL-21 Is Indispensable for Hypoxia-Induced M2 Polarization of Alveolar Macrophages in the Lungs. We hypothesized that IL-21, which has been reported to be majorly secreted from Th17 cells in mice, might play a role in the hypoxia-induced generation of M2 macrophages in the lung. IL-21 treatment of alveolar macrophages isolated from BALF significantly up-regulated the mRNA levels of M2 signature genes, such as *Fizz1*, *Arg1*, and *Cxcl12* (Fig. 5A–C), but had no effect on the mRNA levels of M1 signature genes, including *Nos2*, *Il-12 β* , and *Tnf- α* (Fig. S3D–F). These results indicate that IL-21 specifically induces the M2 polarization of alveolar macrophages.

We next examined the effect of IL-21R deletion on the hypoxia-induced up-regulation of M2 signature genes, including *Fizz1*, *Arg1*, and *Cxcl12*, in the alveolar macrophages isolated from the BALF after exposure to hypoxia for 4 d. All these genes were significantly up-regulated in the alveolar macrophages isolated from WT mice but not in those from IL-21RKO mice (Fig. 5D–F). Similarly, *Fizz1* protein expression was increased

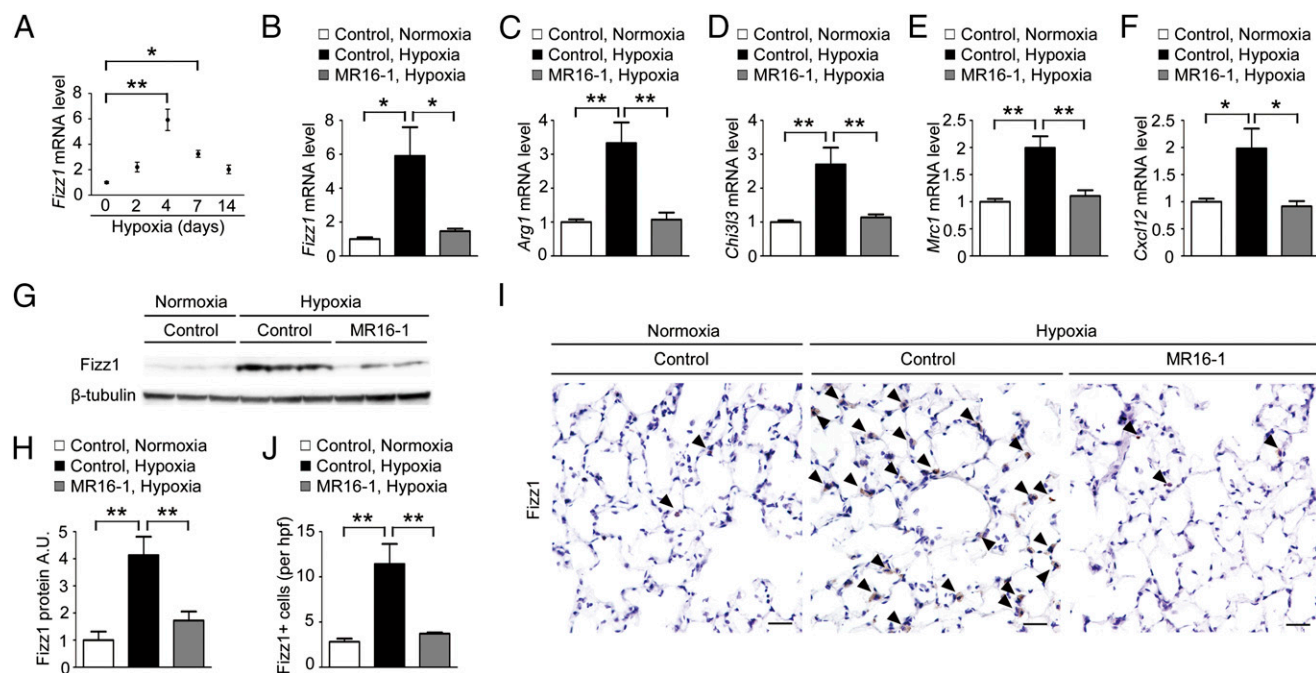


Fig. 4. IL-6 blockade ameliorates the hypoxia-induced generation of M2 macrophages in the murine lung. (A) qRT-PCR analysis of *Fizz1* mRNA expression in the alveolar macrophages isolated from the BALF of C57BL/6 WT mice after hypoxia exposure. The results are pooled data from three independent experiments with 6 mice per group. (B–F) qRT-PCR analysis of M2 macrophage marker genes, including *Fizz1* (B), *Arg1* (C), *Chi3l3* (D), *Mrc1* (E), and *Cxcl12* (F) in the alveolar macrophages isolated from mice treated with control antibody or MR16-1 after exposure to hypoxia or normoxia for 4 d ($n = 6$). (G) Western blot analysis of Fizz1 in lung homogenates from mice treated with control antibody or MR16-1 after exposure to hypoxia or normoxia for 1 wk ($n = 6$). (H) Relative Fizz1 protein levels (normalized to β -tubulin level) compared with normoxic mice treated with control antibody. (I) Representative Fizz1 immunostaining of the alveolar areas to detect the accumulation of M2 macrophages (arrowheads) in mice treated with control antibody or MR16-1 after exposure to hypoxia or normoxia for 1 wk ($n = 5$). (Scale bars: 25 μ m.) (J) Quantification of Fizz1⁺ cells in the alveolar areas. Data shown are the mean number of positive cells per high-power field \pm SEM; * $P < 0.05$, ** $P < 0.01$ calculated using ANOVA.

in the lungs of WT mice but not in those of IL-21RKO mice after exposure to hypoxia for 1 wk (Fig. 5 G and H). In contrast, M1 signature gene expression was comparable in the WT and IL-21RKO mice after exposure to hypoxia (Fig. S3 G–I). Consistent with these findings, the hypoxia-induced generation of M2 macrophages in the lung was inhibited significantly by treatment with an anti-IL-21 neutralizing antibody but not by treatment with a control antibody (Fig. 5 I and J). Collectively, these findings suggest that IL-21 is essential for hypoxia-induced M2 macrophage polarization in the lung.

IL-21-Induced M2 Macrophage Polarization Is Required for the Hypoxia-Induced Proliferation of PSMCs in the Lung. We next investigated the molecular mechanism by which the IL-6/IL-21–signaling axis drives the proliferation of PSMCs after hypoxia exposure. Treatment with IL-6, sIL-6R, or both did not promote the proliferation of human PSMCs (HPASMCs), but treatment with FBS (5%) did (Fig. S5A). Similarly, treatment with IL-21 did not increase the proliferation of HPASMCs (Fig. S5B). Intriguingly, treatment with the conditioned medium of the alveolar macrophages that had been cultivated with IL-21 promoted HPASMC proliferation (Fig. 5K), indicating that soluble factors secreted by the M2 macrophages may promote HPASMC proliferation. CXCL12 is a chemokine that stimulates vascular smooth muscle cell proliferation by binding to its receptor CXCR4 (23). Treatment with a selective CXCR4 antagonist, AMD3100, significantly attenuated the proliferative effect of the alveolar macrophage-conditioned medium on the HPASMCs (Fig. 5L).

We next examined the effect of IL-21 blockade on the in vivo hypoxia-induced proliferation of PSMCs. Hypoxia exposure significantly increased the number of anti-Ki67 antibody–positive PSMCs in the lungs of WT mice but not in the lungs of IL-

21RKO mice (Fig. S5 C and D). Consistent with this finding, hypoxia exposure significantly increased the number of anti-phospho-histone H3 (p-HH3) antibody–positive PSMCs in the lungs of mice treated with control antibody but not in those treated with the anti-IL-21 neutralizing antibody (Fig. 5 M and N). Taken together, these data suggest that IL-21 plays a critical role in the hypoxia-induced proliferation of PSMCs in association with M2 macrophage skewing (see Fig. 7).

Increased Expression of IL-21 and M2 Macrophage Markers in the Lungs of Patients with IPAH. To validate the clinical significance of our experimental findings, we performed immunohistochemical analyses of the lung tissues from patients with IPAH undergoing lung transplantation. Notably, an excessive infiltration of IL-21⁺ cells was detected in the adventitia, obliterative intimal proliferative lesions, and plexiform lesions of the remodeled pulmonary arteries (Fig. 6 A and B), and more moderate infiltration was detected in the alveolar areas of the lungs of IPAH patients (Fig. 6C). In contrast, IL-21⁺ cell infiltration was barely detected in the lungs of the control patient (Fig. 6 A–C). We also observed both Arg1⁺ and MRC1⁺ cells in all layers of the remodeled pulmonary arteries and alveolar areas examined in the lungs from patients with IPAH but not in the tissue from control patients (Fig. 6 D–I). Together, these findings strongly suggest that the IL-6/IL-21–signaling axis is essential for the pathogenesis of human PAH in association with M2 macrophage polarization (Fig. 7).

Discussion

Here, we demonstrate that IL-6 blockade by MR16-1 effectively prevented HPH in mice. IL-6 exhibited critical roles in the hypoxia-induced accumulation of Th17 cells and M2 macrophages in the lungs and in the up-regulation of IL-17 and IL-21, which are

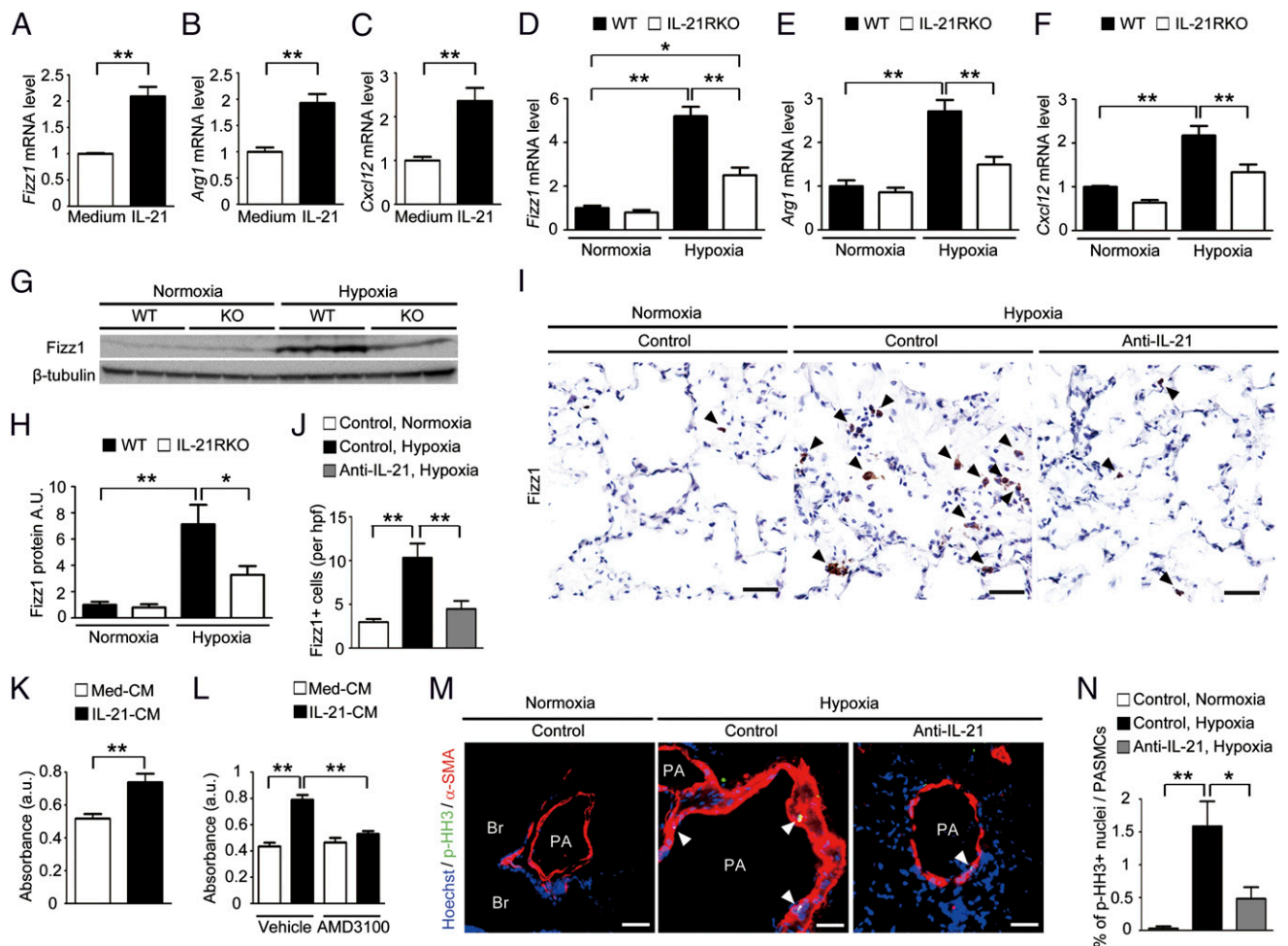


Fig. 5. IL-21-induced M2 macrophage polarization is associated with hypoxia-induced pulmonary vascular remodeling. (A–C) qRT-PCR analysis of M2 macrophage markers in IL-21-treated primary mouse alveolar macrophages. (D–F) qRT-PCR analysis of M2 macrophage markers in alveolar macrophages isolated from WT and IL-21RKO mice after exposure to hypoxia for 4 d ($n = 6$). (G and H) Fizz1 Western blot analysis of lung homogenates from mice exposed to hypoxia for 1 wk ($n = 6$). (I) Fizz1 immunostaining of lung sections from mice treated with control or an anti-IL-21 neutralizing antibody after exposure to hypoxia for 1 wk ($n = 5$). (J) Quantification of Fizz1⁺ cells in the alveolar areas. Values are the mean number of Fizz1⁺ cells per high-power field \pm SEM. (K) Effects of the conditioned medium (CM) obtained from primary mouse alveolar macrophages cultivated with IL-21 on the proliferation of HPASMCs. (L) Inhibitory effect of AMD3100 on the proliferation of HPASMCs cultured with the conditioned medium of IL-21-treated primary mouse alveolar macrophages; Med-CM, conditioned medium of control alveolar macrophages. (M) p-HH3 (green) and α -smooth muscle actin (α -SMA) (red) immunostaining of lung sections from mice treated with an anti-mouse IL-21 neutralizing antibody after exposure to hypoxia for 1 wk ($n = 5$). (N) Percentage of p-HH3⁺ nuclei (arrowheads) in the PASMCs. (Scale bars: 40 μ m.) Br, bronchus; PA, pulmonary artery. Values shown are the mean \pm SEM; * $P < 0.05$, ** $P < 0.01$ calculated using ANOVA.

produced mainly by Th17 cells. Although treating mice with a neutralizing IL-17A antibody did not affect HPH development, IL-21R-deficient mice were resistant to HPH and showed no significant accumulation of M2 macrophages in the lungs. Intriguingly, IL-21 was found to promote the M2 polarization of alveolar macrophages in vitro. We also found enhanced expression of IL-21 and M2 macrophage markers in the lung specimens of IPAH patients. Collectively, these findings suggest that the IL-6/IL-21-signaling axis promotes the pathogenesis of PAH, in concert with the accumulation of M2 macrophages in the lungs (Fig. 7).

IL-6 blockade significantly inhibited the Th17-cell accumulation in the lungs after hypoxia exposure (Fig. 2). IL-6, in cooperation with TGF- β , is reported to be critical for the differentiation of Th17 cells from naive CD4⁺ T cells (15, 24, 25). A humanized monoclonal anti-IL-6R antibody, tocilizumab, is an efficacious therapeutic for patients with rheumatoid arthritis (26, 27). Mechanistically, the protective effect of IL-6 blockade in autoimmune arthritis is attributed primarily to the inhibition of Th17 differentiation (28, 29). Similarly, IL-6 blockade inhibits the induction of

Th17 and Th1 cells in an animal model of multiple sclerosis (30). A recent clinical study reported that genes related to IL-17 signaling were up-regulated significantly in lung specimens from patients with IPAH undergoing lung transplantation (31). In addition, previous clinical studies reported that the IL-6 level in the serum or plasma correlated with the severity of pulmonary hypertension in the patients with IPAH and chronic obstructive pulmonary disease (9, 10, 32). Collectively, these findings indicate that the IL-6/Th17-signaling axis plays a key role in the pathogenesis of inflammatory diseases, including PAH.

IL-6 blockade by MR16-1 also abrogated the hypoxia-induced M2 macrophage polarization in the lungs (Fig. 4). M2 macrophage polarization has been implicated in the pathogenesis of pulmonary hypertension (19, 33, 34), and immunization with certain antigens evokes pulmonary arterial muscularization along with a Th2 response and the subsequent polarization of M2 macrophages (33). Notably, the lung-specific transgenic overexpression of heme oxygenase-1 effectively inhibits the hypoxia-induced up-regulation of inflammatory cytokines (including IL-6), M2 macrophage

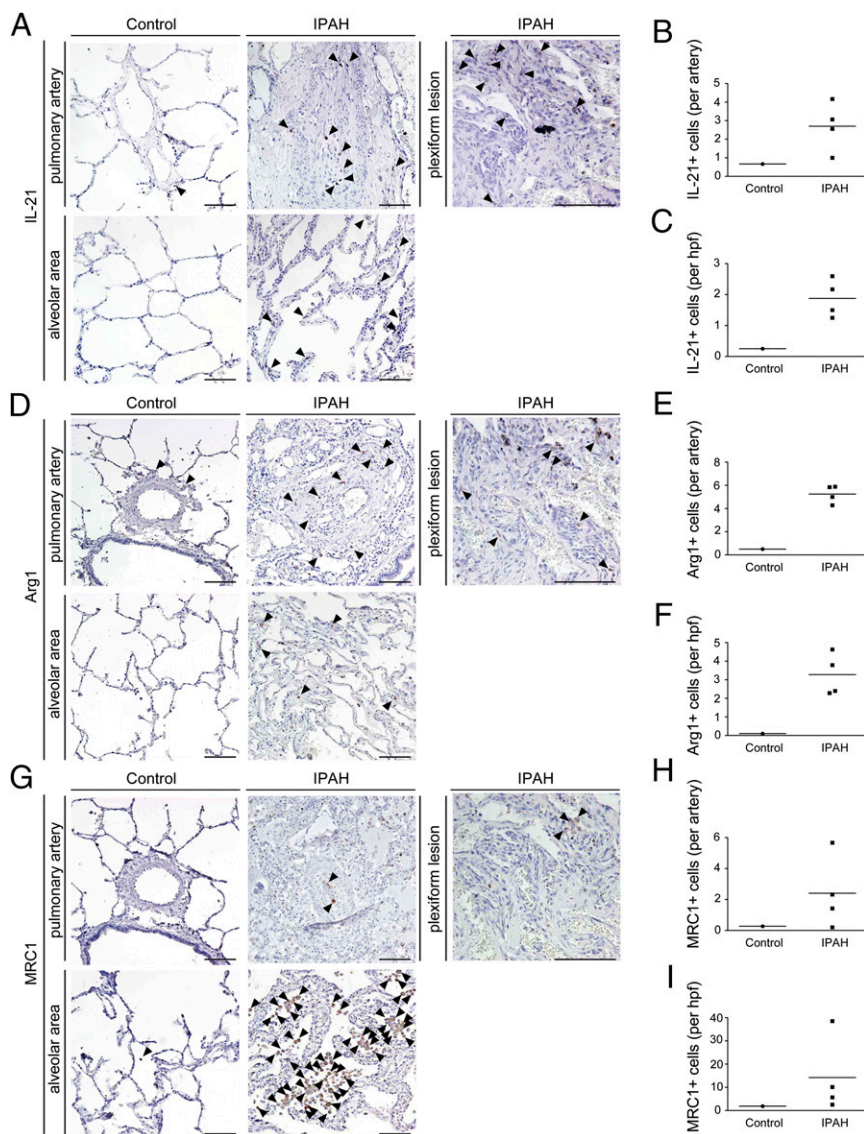


Fig. 6. Significantly enhanced expression of IL-21 and M2 macrophage markers is detected in the lungs of IPAH patients who underwent lung transplantation. (A, D, and G) Representative IL-21, Arg1, and MRC-1 immunostaining of the pulmonary artery, plexiform lesion, and alveolar area from the lungs of a control patient and patients with IPAH. Arrowheads indicate IL-21⁺ (A), Arg1⁺ (D), and MRC-1⁺ (G) cells. (Scale bars: 100 μ m). (B, E, and H) The numbers of IL-21⁺ (B), Arg1⁺ (E), and MRC-1⁺ (H) cells around one pulmonary artery of a control patient and IPAH patients. The horizontal line in the graph indicates the mean number in each group. (C, F, and I) The numbers of IL-21⁺ (C), Arg1⁺ (F), and MRC-1⁺ (I) cells per high-power field in the alveolar areas of the control patient and IPAH patients. The horizontal line in the graph indicates the mean number in each group.

accumulation, and the subsequent development of pulmonary hypertension (19, 34). Taken together, these data suggest that IL-6 blockade may prevent HPH, at least in part, by inhibiting M2 macrophage polarization.

IL-6 is reported to induce the up-regulation of IL-21 in naive and memory CD4⁺ T cells (35, 36). In addition, IL-21 also is produced by Th17 cells and drives Th17 differentiation in an autocrine manner (36–38). Here we found that hypoxia exposure induced transient expression of IL-6 and prolonged expression of IL-17 and IL-21 in the lungs (Figs. 1A, 2A, and 3A). The prolonged induction of IL-17 and IL-21 may result from the autocrine production of IL-21 by Th17 cells. Taken together, these findings indicate that IL-21 may be critical for the sustained inflammation that promotes the development of pulmonary hypertension.

The involvement of IL-21 in M2 macrophage polarization has been reported previously (39, 40). In a colitis-associated colon cancer model, IL-21RKO mice show less M2 macrophage in-

filtration into tumors than WT model mice (40). IL-21RKO mice also exhibit a markedly reduced expression of several M2 macrophage-related genes in the lungs when infected with parasites, as compared with WT mice (40). Here, we found that IL-21RKO mice were resistant to HPH and failed to accumulate M2 macrophages in the lungs after hypoxia exposure, unlike WT mice (Figs. 3H–L and 5D–F). Furthermore, we found that the expression levels of IL-21 and of M2 macrophage signature genes were up-regulated in the lungs of IPAH patients (Fig. 6). This last finding supports the clinical significance of the link between the IL-6/IL-21–signaling axis and the pathogenesis of PAH suggested by the results of our animal studies.

In conclusion, our findings indicate that the IL-6/IL-21–signaling axis plays a critical role in the pathogenesis of PAH and suggest that this signaling axis may yield potential therapeutic targets for treating patients with PAH.

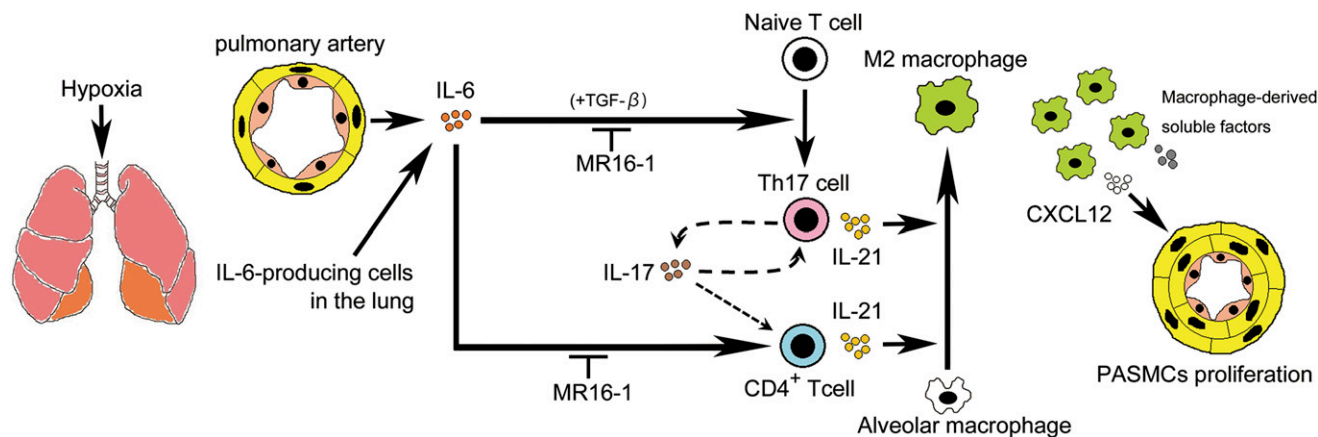


Fig. 7. Schematic illustration of the development of PAH through the IL-6/Th17/IL-21–signaling axis. Hypoxia induces the up-regulation of IL-6 in the PAECs (orange) and PSMCs (yellow). IL-6 promotes the differentiation of Th17 cells from naive T cells, presumably in cooperation with TGF- β in the lung. IL-17, derived mainly from Th17 cells, is partly responsible for the production of IL-21 in these cells. IL-21, secreted from CD4⁺ T cells, including Th17 cells, promotes macrophage skewing toward the M2 phenotype in the alveolar macrophages. M2 macrophages positively regulate the hypoxia-induced proliferation of PSMCs by releasing soluble factors such as CXCL12. Taken together, these data show that IL-21 plays a critical role in the pathogenesis of PAH in concert with M2 macrophage polarization downstream of the IL-6/IL-21–signaling axis and may be a potential therapeutic target for treating patients with PAH.

Materials and Methods

Full experimental procedures and associated references are available in *SI Materials and Methods*.

Animals. All experiments were carried out under the guidelines of the Osaka University Committee for Animal and Recombinant DNA Experiments and the local Animal Ethics Committee of the National Cerebral and Cardiovascular Center Research Institute (Osaka) and also were approved by the Institutional Review Board of Osaka University and the National Cerebral and Cardiovascular Center Research Institute. Male C57BL/6 8-wk-old mice (average body weight: 21.4 g) purchased from Japan SLC, Inc. were used in the experiments. In most of the experiments examining the effect of IL-6 blockade, the mice were divided into four groups: normoxic control antibody group ($n = 8$), normoxic MR16-1 group ($n = 8$), hypoxic control antibody group ($n = 10$), and hypoxic MR16-1 group ($n = 12$). IL-21RKO mice were kindly provided by Warren J. Leonard, National Heart, Lung, and Blood Institute, Bethesda (22). IL-21RKO heterozygous mice were intercrossed, and male 8-wk-old littermates of WT and IL-21RKO mice were used in the following experiments. The average body weight of the male IL-21RKO mice was 21.5 g. In most of the experiments examining the effect of IL-21R deficiency, the mice were divided into four groups: normoxic WT group ($n = 5$), normoxic IL-21RKO group ($n = 5$), hypoxic WT group ($n = 10$), and hypoxic IL-21RKO group ($n = 9$). All mice were housed on a 12-h light/12-h dark cycle at $24 \pm 1^\circ\text{C}$ and were given standard mouse food and water ad libitum. The mice either were housed under standard normoxic conditions or were housed continuously in a hypoxic chamber (10% O_2) for up to 4 wk, except for a 5-min interval twice a week when the chamber was cleaned. The hypoxic gas mixture was delivered continuously to the chamber at a flow rate of ~ 1 L/min. After chronic hypoxic exposure, the mice were subjected to hemodynamic recording and were killed for pathological analysis of the heart and lungs.

Treatment of Mice with Neutralizing Antibodies. MR16-1, a rat IgG1 monoclonal neutralizing antibody against murine IL-6R, was kindly provided by Chugai Pharmaceutical Co. (41). To determine the effect of the MR16-1-mediated blockade of IL-6, mice were i.v. injected with 2 mg of MR16-1 or purified rat nonimmune isotype control IgG (MP Biomedicals) just before exposure to hypoxia or normoxia and subsequently were injected i.p. with 0.5 mg of MR16-1 or control IgG, respectively, once a week. To block IL-17A, mice were injected i.p. with 200 μg of a neutralizing anti-mouse IL-17A monoclonal antibody, MAB421 (R&D Systems) or isotype control IgG on days $-1, 0, 1, 2, 3, 4, 7, 10, 13, 16, 19, 22,$ and 25 after hypoxia exposure was initiated. To block IL-21, mice were injected i.p. with 100 μg of a neutralizing anti-mouse IL-21 monoclonal antibody (FFA21; eBioscience) or isotype control IgG on days $-1, 0, 1, 2, 3,$ and 4 after exposure to hypoxia or normoxia was initiated.

Surgical Preparation and Blood Pressure Measurements. Mice were anesthetized with pentobarbital sodium (60 mg/kg i.p.) and an analgesic agent,

butorphanol tartrate (0.1–0.4 mg/kg i.p.). Supplementary doses of pentobarbital (15–20 mg·kg⁻¹·h⁻¹ i.p.) and butorphanol tartrate (0.03–0.05 mg·kg⁻¹·h⁻¹ i.p.) were administered periodically to maintain a surgical level of anesthesia. Throughout the procedure, the body temperature was maintained at $37\text{--}38^\circ\text{C}$ using a rectal thermistor coupled with a thermostatically controlled heating pad. The trachea was cannulated, and the lungs were ventilated with a mouse ventilator (Minivent Type 845; Harvard Apparatus) (42). The inspired gas was enriched with oxygen, and the ventilator settings were adjusted (tidal volume 6 $\mu\text{L/g}$; frequency $\sim 170\text{--}190/\text{min}$). A polyethylene tube was inserted into the right external jugular vein and advanced into the right ventricle (RV) to measure right ventricular pressure (RVP). RVP signals were detected by a pressure transducer (MLT0670; AD Instruments), and the signals were relayed to pressure amplifiers (ML117; AD Instruments) and then were sampled continuously with a PowerLab system (AD Instruments) and recorded on a computer using Chart software (AD Instruments) (42). Heart rate (HR) was derived from the right ventricular systolic peaks and was typically between 300 and 500 beats/min (bpm) under these conditions. If the HR fell below 300 bpm, the measurements were excluded from the analysis. Systemic arterial blood pressure was obtained noninvasively from conscious mice using a computerized tail-cuff system (BP-98A-L; Softron) as described previously (43).

Western Blot Analysis. Frozen lungs were homogenized in 50 mM HEPES, 100 mM sodium fluoride, 2 mM sodium orthovanadate, 4 mM EDTA, 1% Tween-20, 0.1% SDS, and Complete protease inhibitor mixture (Roche Applied Science) using a Polytron homogenizer (PT 10-35GT; Kinematica) as described previously (44). The precleared lysates then were resolved by SDS/PAGE and subjected to Western blot analysis using a standard procedure with the following antibodies: anti-pSTAT3-Tyr705 (clone D3A7; Cell Signaling), anti-STAT3 (clone 79D7; Cell Signaling), anti-RELM alpha (Fizz1) (ab39626; Abcam), anti-IL-17A (sc-52567; Santa Cruz), and anti-IL-21 (MAB594; R&D Systems). An anti- β -tubulin antibody (T5201; Sigma-Aldrich) was used as the internal control. The blots were developed using HRP-coupled secondary antibodies (Cell Signaling Technology) and the ECL system (GE Healthcare).

Morphometric Analysis. After hemodynamic recording, the mice were killed by anesthesia overdose, and the heart was excised. The atria were removed, and the RV wall was separated from the left ventricle (LV) and septum. The tissues were blotted, weighed, and their weights normalized to a 100-g body weight. Fulton's index, the ratio of RV to LV + septum weight [$\text{RV}/(\text{LV} + \text{S})$] was used as an index of right ventricular hypertrophy (45). The lungs then were harvested for histological and immunohistochemical analyses. The pulmonary artery and trachea were perfused with 4% (wt/vol) paraformaldehyde (PFA) at constant pressure (100 cm H_2O for the pulmonary artery and 25 cm H_2O for the trachea) to distend fully the pulmonary blood vessels and airway, respectively. Excised lungs were fixed in 4% PFA overnight at 4°C and then were embedded in paraffin and cut into 4- μm -thick sections. For pulmonary

vascular morphometry, paraffin-embedded lung sections were subjected to elastic Van Gieson staining. Images of arteries were captured with a fluorescence microscope (BZ-9000; Keyence). Morphometry was performed on lung sections obtained from five or six randomly chosen animals in each treatment group. Pulmonary remodeling was assessed by the percent wall thickness of parenchymal pulmonary arteries classified into the small arteries (terminal bronchioles) and arterioles (acini or alveolar ducts). The percent wall thickness was the medial wall thickness (the distance between the internal and external lamina) $\times 2$ divided by the diameter of the vessel (the distance between the external lamina) $\times 100$. For vessels with a single elastic lamina, the distance between the elastic and endothelial basement membrane was measured. Medial thickness was analyzed only for sectioned vessels exhibiting an approximately circular profile. The diameter of pulmonary arteries was determined by Image J software (National Institutes of Health). The percent wall thickness was calculated for at least 10 small pulmonary arteries and arterioles for each mouse.

Lung Specimens from Patients with IPAH. All the experiments using human specimens were approved by the Institutional Review Board of Osaka University, Suita, Japan. The lung tissues were obtained from four patients with IPAH undergoing lung transplantation and from a control patient undergoing surgery for lung cancer at a site far away from the tumor margins. All lung specimens were procured at Osaka University Hospital. Before surgery, all patients provided written consent for the use of their lung tissues for biomedical research. The resected lung tissues were fixed in 10% PFA. Patient characteristics are shown in Table S3.

Histological and Immunohistochemical Analyses of the Pulmonary Vasculatures.

For the immunohistochemical analyses of murine lung tissues, samples were fixed in 4% PFA/PBS for 1 h, cryoprotected with PBS containing 5–20% sucrose, frozen in OCT compound (Sakura), and cut into 10- μ m-thick cryosections as described previously (46). Human lung samples, which were formaldehyde-fixed and paraffin-embedded, were cut into 5- μ m-thick sections, deparaffinized, and rehydrated. The human sections were subjected to antigen retrieval either by heat induction in 10 mM sodium citrate buffer, pH 6.0, or by proteinase K digestion for 3 min. All lung sections then were washed in PBS, treated with 1% hydrogen peroxide in methanol for 30 min, incubated in blocking solution containing either 1% BSA or 5% skim milk in PBS and 0.1% Triton-X (PBST) for 1 h, and incubated with primary antibody in PBST overnight at 4 °C or 25 °C. The following primary antibodies were used for immunostaining: anti-RELM alpha (Fizz1) (1:100 dilution; ab39626; Abcam); anti-IL-6 (1:200 dilution; ab6672; Abcam); anti-p-HH3 (Ser10) (1:100 dilution; 06-570; Upstate); anti-Ki67 (1:200 dilution; ab16667; Abcam); anti-Actin, alpha-Smooth Muscle-Cy3 (1:200 dilution; C6198; Sigma-Aldrich); anti-Arg1 (1:1,000 dilution; HPA024006; Sigma-Aldrich); anti-mannose receptor (MRC1) (1:1,000 dilution; ab64693; Abcam); and anti-IL-21 (1:200 dilution; NBP1-02706; Novus). Next, the sections were washed in PBST and incubated with fluorescence-conjugated (1:200 dilution; Alexa Fluor 488- or 546-coupled; Invitrogen) or HRP-coupled (1:200 or 1:400 dilution; 7074; Cell Signaling Technology) secondary antibodies for 1 h at room temperature, and, if necessary, were visualized using 3,3'-diaminobenzidine substrate (Sigma). Images were acquired with a fluorescence microscope (BZ-9000; Keyence). Negative control sections for the immunohistochemical experiments received identical treatment except for exposure to the primary antibodies and showed no specific staining. Fizz1⁺ cells were counted in 10–20 high-power fields (magnification: 400 \times) per mouse. p-HH3⁺ cells and Ki67⁺ cells were counted in at least 10 pulmonary arteries for each mouse. Arg1⁺, MRC1⁺, and IL-21⁺ cells were counted in at least 10 pulmonary arteries or at least 10 high-power fields (magnification: 200 \times) in the alveolar area from each human sample.

Flow Cytometry Analysis. Lung tissue was incubated directly for 40 min to 1 h at 37 °C in DMEM containing collagenase and DNase1 (1 U/mL) (Takara). The tissue suspensions then were pressed through a 40- μ m mesh, pelleted, resus-

pended in PBS-F (PBS containing 2% FBS), and the cells were washed twice with PBS-F. The cells were preincubated with an antibody to CD16/32 to block Fc γ receptors and then were washed and incubated with the indicated fluorophore-conjugated antibody (CD4) for 30 min in a total volume of 100 μ L PBS-F. For intracellular cytokine staining, the cells first were stimulated for 5 h in complete medium in the presence of 25 ng/mL phorbol12-myristate13-acetate, 1 μ g/mL ionomycin, and 10 μ g brefeldin A (Sigma-Aldrich) and then were stained for CD4, followed by fixation and permeabilization using the Mouse Foxp3 Buffer Set (BD Pharmingen) according to the manufacturer's instructions. After two washes, the cells were stained for 30 min on ice with fluorophore-conjugated antibodies (anti-IFN- γ , anti-IL-4, anti-IL-17A, anti-IL-21) or the appropriate isotype control antibodies. The purity of the cells isolated from BALF was assessed by using the fluorophore-conjugated antibodies against CD45, F4/80, and CD11c or the appropriate isotype control antibodies. Dead cells were excluded by propidium iodide. The cells then were analyzed on a FACSCanto (BD Biosciences), followed by analysis with FlowJo software (Tri-Star). The following antibodies were used for flow cytometry analyses: FITC-conjugated anti-CD4 (RM4-5), PE-conjugated anti-IFN- γ (XMG1.2), APC-conjugated anti-IL-4 (11B11), APC-conjugated anti-IL-17A (eBio17B7), PE-conjugated anti-IL-21 (mhalx21), and APC-conjugated anti-F4/80 (BM8) from eBioscience and PE-conjugated anti-CD45 (30-F11) and FITC-conjugated anti-CD11c (HL3) from BD Biosciences.

qRT-PCR. Total RNA from the mouse lung or alveolar macrophages was extracted using TRIzol reagent (Invitrogen). qRT-PCR was carried out using the QuantiFast SYBRGreen RT-PCR kit (Qiagen) as described previously (47). For each reaction, 80 ng of total RNA was transcribed for 10 min at 50 °C, followed by a denaturing step at 95 °C for 5 min and 40 cycles of 10 s at 95 °C and 30 s at 60 °C. Fluorescence data were collected and analyzed using an ABI PRISM 7900HT. The following primers were used: *Gapdh*: 5'-TCTCCACACCTATGGTGCAA-3', 5'-CAAGAAACAGGGGAGCTGAG-3'; *Fizz1*: 5'-CCCTTCTCATCTGCATCTCC-3', 5'-AGGAGGCCCATCTGTTTCATA-3'; *Arg1*: 5'-GTGAA-GAAGCCACGGTCTGT-3', 5'-CTGGTTGTGAGGGGAGTGT-3'; *Chi3l3*: 5'-CCCA-CGAGGAAATGACACAG-3', 5'-GAGGAAATGCTCTGTGTGA-3'; *Mrc1*: 5'-CG-CGAGGCAATTTTAAATCT-3', 5'-ATTTGCATTGCCAGTAAGG-3'; *Cxcl12*: 5'-GGTTC-TTCGAGAGCCACATC-3', 5'-TAATTTTCGGTCAATGACACA-3'; *Il17a*: 5'-TCCAGAA-GGCCCTCAGACTA-3', 5'-CTCGACCCTGAAAGTGAAGG-3'; *Rorc*: 5'-AACCCAGG-CATCTGAAGCTTG-3', 5'-CGTAGAAGGTCCTGCTGCTG-3'; *Cxcl1*: 5'-GCGCATC-GCCAATGAGCTG-3', 5'-TCTGAACCAAGGGAGCTTCA-3'; *Cxcl5*: 5'-CTGCCCTT-CCTCAGTCATA-3', 5'-TGGATCCAGACAGACCTCCT-3'; *Il21*: 5'-GGACAGTGGCC-ATAAATCA -3', 5'-CAGGTTTGTATGGCTTGAAGT -3'; *Il6*: 5'-TGTCATGCGCAAT-TGAT-3', 5'-GGTACTCCAGAAGACAGGAGCA-3'; *Nos2*: 5'-GCGCATCAGTCAG-CAGAA-3', 5'-TGTTGTCATTGGAAGTGAAGC-3'; *Il12b*: 5'-AGGTCACACTGGACCA-AAGG-3', 5'-AGGGTACTCCAGCTGACCT-3'; *Tnf- α* : 5'-TGCCTATGTCTAGCCTCTTC-3', 5'-GGTCTGGCCATAGAACTGA-3'.

Statistics. All data are expressed as the mean \pm SEM. Differences among multiple groups were compared by one-way ANOVA followed by a post hoc comparison tested with Scheffé's method. The Student's *t* test was used to analyze differences between two groups. *P* < 0.05 was considered statistically significant.

ACKNOWLEDGMENTS. We thank Yuka Yoshimoto and Yumi Yanagisawa for secretarial assistance; Kaori Yamamoto and Manami Sone (National Cerebral and Cardiovascular Research Center) for technical assistance; Yoshito Takeda, Yingji Jin (Osaka University), Yasunobu Arima (Hokkaido University), Hatsue Ueda, Naoki Mochizuki (National Cerebral Cardiovascular Research Center), Susumu Nakae, and Tomokazu Sumida (University of Tokyo) for helpful discussions and suggestions; Warren J. Leonard (National Heart, Lung, and Blood Institute) for providing IL-21RKO mice; and Chugai Pharmaceutical Co. for providing the anti-IL-6R antibody MR16-1. This work was supported in part by Grant KAKENHI-25670386 from the Ministry of Education, Science, Sports and Culture of Japan (to Y.N.) and by a grant from Precursory Research for Embryonic Science and Technology, Japan Science Technology Agency (to Y.N.).

- Pietra GG, et al. (2004) Pathologic assessment of vasculopathies in pulmonary hypertension. *J Am Coll Cardiol* 43(12, Suppl S):255–325.
- Rabinovitch M (2012) Molecular pathogenesis of pulmonary arterial hypertension. *J Clin Invest* 122(12):4306–4313.
- Dorfmueller P, Perros F, Balabanian K, Humbert M (2003) Inflammation in pulmonary arterial hypertension. *Eur Respir J* 22(2):358–363.
- Schermlay RT, Ghofrani HA, Wilkins MR, Grimminger F (2011) Mechanisms of disease: Pulmonary arterial hypertension. *Nat Rev Cardiol* 8(8):443–455.
- Tuder RM, Groves B, Badesch DB, Voelkel NF (1994) Exuberant endothelial cell growth and elements of inflammation are present in plexiform lesions of pulmonary hypertension. *Am J Pathol* 144(2):275–285.
- Tuder RM, Voelkel NF (1998) Pulmonary hypertension and inflammation. *J Lab Clin Med* 132(1):16–24.
- Kishimoto T (2006) Interleukin-6: Discovery of a pleiotropic cytokine. *Arthritis Res Ther* 8(Suppl 2):S2.
- Kishimoto T, Akira S, Taga T (1992) Interleukin-6 and its receptor: A paradigm for cytokines. *Science* 258(5082):593–597.
- Humbert M, et al. (1995) Increased interleukin-1 and interleukin-6 serum concentrations in severe primary pulmonary hypertension. *Am J Respir Crit Care Med* 151(5):1628–1631.
- Soon E, et al. (2010) Elevated levels of inflammatory cytokines predict survival in idiopathic and familial pulmonary arterial hypertension. *Circulation* 122(9):920–927.

11. Steiner MK, et al. (2009) Interleukin-6 overexpression induces pulmonary hypertension. *Circ Res* 104(2):236–244.
12. Savale L, et al. (2009) Impact of interleukin-6 on hypoxia-induced pulmonary hypertension and lung inflammation in mice. *Respir Res* 10:6.
13. Iwakura Y, Ishigame H, Saijo S, Nakae S (2011) Functional specialization of interleukin-17 family members. *Immunity* 34(2):149–162.
14. Korn T, Bettelli E, Oukka M, Kuchroo VK (2009) IL-17 and Th17 Cells. *Annu Rev Immunol* 27:485–517.
15. Bettelli E, et al. (2006) Reciprocal developmental pathways for the generation of pathogenic effector TH17 and regulatory T cells. *Nature* 441(7090):235–238.
16. Biswas SK, Mantovani A (2010) Macrophage plasticity and interaction with lymphocyte subsets: Cancer as a paradigm. *Nat Immunol* 11(10):889–896.
17. Mosser DM, Edwards JP (2008) Exploring the full spectrum of macrophage activation. *Nat Rev Immunol* 8(12):958–969.
18. Wynn TA, Chawla A, Pollard JW (2013) Macrophage biology in development, homeostasis and disease. *Nature* 496(7446):445–455.
19. Vergadi E, et al. (2011) Early macrophage recruitment and alternative activation are critical for the later development of hypoxia-induced pulmonary hypertension. *Circulation* 123(18):1986–1995.
20. Tanaka T, Narazaki M, Kishimoto T (2012) Therapeutic targeting of the interleukin-6 receptor. *Annu Rev Pharmacol Toxicol* 52:199–219.
21. Liu SM, King C (2013) IL-21-producing Th cells in immunity and autoimmunity. *J Immunol* 191(7):3501–3506.
22. Ozaki K, et al. (2002) A critical role for IL-21 in regulating immunoglobulin production. *Science* 298(5598):1630–1634.
23. Takeda Y, et al. (2011) Macrophage skewing by Phd2 haplodeficiency prevents ischaemia by inducing arteriogenesis. *Nature* 479(7371):122–126.
24. Mangan PR, et al. (2006) Transforming growth factor-beta induces development of the T(H)17 lineage. *Nature* 441(7090):231–234.
25. Veldhoen M, Hocking RJ, Atkins CJ, Locksley RM, Stockinger B (2006) TGFbeta in the context of an inflammatory cytokine milieu supports de novo differentiation of IL-17-producing T cells. *Immunity* 24(2):179–189.
26. Choy EH, et al. (2002) Therapeutic benefit of blocking interleukin-6 activity with an anti-interleukin-6 receptor monoclonal antibody in rheumatoid arthritis: A randomized, double-blind, placebo-controlled, dose-escalation trial. *Arthritis Rheum* 46(12):3143–3150.
27. Nishimoto N, et al. (2004) Treatment of rheumatoid arthritis with humanized anti-interleukin-6 receptor antibody: A multicenter, double-blind, placebo-controlled trial. *Arthritis Rheum* 50(6):1761–1769.
28. Fujimoto M, et al. (2008) Interleukin-6 blockade suppresses autoimmune arthritis in mice by the inhibition of inflammatory Th17 responses. *Arthritis Rheum* 58(12):3710–3719.
29. Iwanami K, et al. (2008) Crucial role of the interleukin-6/interleukin-17 cytokine axis in the induction of arthritis by glucose-6-phosphate isomerase. *Arthritis Rheum* 58(3):754–763.
30. Serada S, et al. (2008) IL-6 blockade inhibits the induction of myelin antigen-specific Th17 cells and Th1 cells in experimental autoimmune encephalomyelitis. *Proc Natl Acad Sci USA* 105(26):9041–9046.
31. Hsu E, et al. (2011) Lung tissues in patients with systemic sclerosis have gene expression patterns unique to pulmonary fibrosis and pulmonary hypertension. *Arthritis Rheum* 63(3):783–794.
32. Chaouat A, et al. (2009) Role for interleukin-6 in COPD-related pulmonary hypertension. *Chest* 136(3):678–687.
33. Daley E, et al. (2008) Pulmonary arterial remodeling induced by a Th2 immune response. *J Exp Med* 205(2):361–372.
34. Minamino T, et al. (2001) Targeted expression of heme oxygenase-1 prevents the pulmonary inflammatory and vascular responses to hypoxia. *Proc Natl Acad Sci USA* 98(15):8798–8803.
35. Dienz O, et al. (2009) The induction of antibody production by IL-6 is indirectly mediated by IL-21 produced by CD4+ T cells. *J Exp Med* 206(1):69–78.
36. Nurieva R, et al. (2007) Essential autocrine regulation by IL-21 in the generation of inflammatory T cells. *Nature* 448(7152):480–483.
37. Korn T, et al. (2007) IL-21 initiates an alternative pathway to induce proinflammatory T(H)17 cells. *Nature* 448(7152):484–487.
38. Zhou L, et al. (2007) IL-6 programs T(H)-17 cell differentiation by promoting sequential engagement of the IL-21 and IL-23 pathways. *Nat Immunol* 8(9):967–974.
39. Pesce J, et al. (2006) The IL-21 receptor augments Th2 effector function and alternative macrophage activation. *J Clin Invest* 116(7):2044–2055.
40. Stolfi C, et al. (2011) Involvement of interleukin-21 in the regulation of colitis-associated colon cancer. *J Exp Med* 208(11):2279–2290.
41. Takagi N, et al. (1998) Blockage of interleukin-6 receptor ameliorates joint disease in murine collagen-induced arthritis. *Arthritis Rheum* 41(12):2117–2121.
42. Sonobe T, et al. (2011) Imaging of the closed-chest mouse pulmonary circulation using synchrotron radiation microangiography. *J Appl Physiol* (1985) 111(1):75–80.
43. Higuchi K, et al. (2012) Endothelial Gab1 deletion accelerates angiotensin II-dependent vascular inflammation and atherosclerosis in apolipoprotein E knockout mice. *Circ J* 76(8):2031–2040.
44. Nakaoka Y, et al. (2007) Gab family proteins are essential for postnatal maintenance of cardiac function via neuregulin-1/ErbB signaling. *J Clin Invest* 117(7):1771–1781.
45. Ogura S, et al. (2013) Oxidative stress augments pulmonary hypertension in chronically hypoxic mice overexpressing the oxidized LDL receptor. *Am J Physiol Heart Circ Physiol* 305(2):H155–H162.
46. Arita Y, et al. (2014) Myocardium-derived angiopoietin-1 is essential for coronary vein formation in the developing heart. *Nat Commun* 5:4552.
47. Shioyama W, et al. (2011) Docking protein Gab1 is an essential component of postnatal angiogenesis after ischemia via HGF/c-met signaling. *Circ Res* 108(6):664–675.